Conversion of CO_2 into valuable products: Engineering the PirC-PGAM switch in cyanobacteria to direct carbon flux into desired products

Nathalie Sofie Becker[1], Franziska Hufnagel[2], Paul Bolay[3], Kevin Otec[2], Tim Orthwein[1], Andreas Kulik[4], Phillipp Fink[1], Claudius Lenz[5], Pia Lindberg[3], Karl Forchhammer[1], Stephan Klähn[2,*]

1 - Interfaculty Institute for Microbiology and Infection Medicine, Organismic Interactions Department, Tübingen University, Auf der Morgenstelle 28, 72076 Tübingen, Germany

2 - Department of Solar Materials Biotechnology, Helmholtz Centre for Environmental Research, Permoserstrasse 15, 04318 Leipzig, Germany

3 - Department of Chemistry - Ångström Laboratory, Uppsala University, Lägerhyddsvägen 1, 752 37 Uppsala, Sweden

4 - Interfaculty Institute of Microbiology and Infection Medicine, Department of Microbial Bioactive Compounds, Tübingen University, Auf der Morgenstelle 28, 72076 Tübingen, Germany

5 - Department of Microbial Biotechnology, Helmholtz Centre for Environmental Research, Permoserstrasse 15, 04318 Leipzig, Germany

Corresponding author: Stephan Klähn, stephan.klaehn@ufz.de

Abstract

Background: In response to rising CO_2 emissions driving global warming, there is an urgent need for a transition toward a sustainable bioeconomy. Photo-biotechnological processes based on oxygenic photosynthesis hold high potential for achieving CO_2 neutrality and in this regard,

cyanobacteria have emerged as promising biocatalysts. Rational metabolic engineering of cyanobacteria depends on a thorough understanding of native regulatory mechanisms governing primary metabolism, which can limit metabolic flux through specific pathways and, consequently, the formation of target products. Recent insights have identified a key regulatory node at the 2,3-bisphosphogylcerate-independent phosphoglycerate mutase (PGAM) reaction, where the metabolic flux from newly fixed carbon is redirected from the Calvin-Benson-Bassham (CBB) cycle towards lower glycolysis. This metabolic valve is controlled by the small inhibitor protein PirC, whose binding to PGAM is determined by the central signal transduction protein PII.

Results: In this study, we exploit the PirC-PGAM interaction as a novel target for regulatory metabolic engineering in the model cyanobacterium *Synechocystis* sp. PCC 6803 (*Synechocystis*). Chassis strains with engineered control of PGAM, defined as PGAM-ON or PGAM-OFF states, were generated using two complementary approaches: tuning *pgam* gene expression and modulating PirC abundance to regulate PGAM activity. The effectiveness of this regulatory engineering strategy was demonstrated by redirecting carbon flux toward two representative, naturally occurring products: sucrose, produced via gluconeogenesis fueled by the Calvin-Benson-Bassham (CBB) cycle, and succinate, an intermediate of the tricarboxylic acid (TCA) cycle. Narrowing the PGAM valve resulted in a threefold increase in sucrose accumulation. In contrast, opening the PGAM valve by relieving PGAM inhibition through *pirC* deletion or separate *pgam* overexpression resulted in up to an 18-fold increase in succinate excretion. Furthermore, similar genetic configurations were applied to enhance production of a heterologous compound, isoprene, derived from pyruvate.

Conclusions: This study establishes the PGAM valve as a tunable control point for the rational re-direction of carbon flux in *Synechocystis* and highlights small regulatory proteins as powerful targets for metabolic engineering. Together, these findings provide proof of concept for an

advanced level of molecular engineering in cyanobacteria and to fully harness their biocatalytic potential in future photosynthesis-driven biotechnological applications.

Keywords: metabolic regulation, metabolic engineering, molecular tools, carbon flux, cyanobacteria

Background

The anthropogenic climate change leads to a growing need for sustainable, i.e. CO_2-neutral, biotechnological processes that may also consider photoautotrophic microorganisms as potential production strains. Cyanobacteria are the only prokaryotes performing oxygenic photosynthesis, which makes use of solar energy to oxidize water and utilize the obtained electrons to assimilate CO_2 [1]. With this, cyanobacteria are dominant primary producers and hence, key players in global biogeochemical cycles [2]. In addition to their environmental impact, they receive growing interest as biocatalysts in photo-biotechnological applications nowadays, e.g. for the sustainable production of value chemicals and fuels [3–5]. To rationally engineer cyanobacteria, e.g. by channeling metabolic fluxes to obtain the maximum yield of a desired chemical product, it is of paramount importance to fully comprehend underlying molecular processes that control primary carbon metabolism [6,7]. Although we are only at the beginning of a full understanding of the regulation of cyanobacterial metabolism, recent research has opened the window into a more comprehensive view on fundamental control principles.

Maintaining the cellular carbon/nitrogen (C/N) homeostasis is one of the most fundamental aspects of cellular physiology. During vegetative growth of autotrophic organisms, it is essential to tightly interconnect CO_2 fixation with N assimilation. To fulfil this task, cyanobacteria use a sophisticated signaling network centered around the pervasive PII sensor protein [8,9]. PII proteins

72 are fundamental for most free-living prokaryotes and plant chloroplasts, where they act as
73 multitasking signal integrators that combine information on the metabolic C/N balance with the
74 energy state of the cell. C/N sensing is achieved through interaction with the metabolite 2-
75 oxoglutarate (2-OG) and energy sensing by competitive binding of ATP or ADP [9]. 2-OG is ideally
76 suited as a status reporter for C/N balance sensing, as it is the C skeleton, into which ammonium
77 is incorporated through the assimilatory reactions catalyzed by the glutamine synthetase-
78 glutamate synthase (GS/GOGAT) cycle [10].

79 The mechanistic details, how the PII proteins interact with effector molecules and transmit this
80 information into distinct conformational states, have been elaborated in great detail [9,11]. Briefly,
81 differential binding of the effector molecules ATP/ADP and 2-OG to the PII protein affects the
82 conformation of flexible loop regions of PII, and depending on these conformational states, PII
83 interacts with its receptor proteins, and by that modulating their activities. By this mechanism, PII
84 controls key enzymes, transporters and small regulatory proteins. For example, PII controls the
85 transcriptional co-activator protein PipX, which the global nitrogen control factor A (NtcA) requires
86 to activate the expression of various N assimilatory genes [12,13]. Furthermore, PII controls the
87 activity of enzymes directly, e.g. acetyl-CoA carboxylase or N-acetyl-L-glutamate-kinase (NAGK),
88 which catalyzes the committed step in arginine synthesis [14–16]. More recently, interactions of
89 PII with small proteins of previously unknown function were also revealed, which in turn provided
90 a plethora of new insights (see below).

91 The interest in small proteins (< 100 amino acids) and their important role in cellular functions has
92 only recently gained more attention [17]. Cyanobacteria appear to provide a paradigm in this
93 regard, as the photosynthetic apparatus contains numerous proteins of less than 50 amino acids
94 [18]. Moreover, several small proteins act as effectors of key enzymes [19] and PII interacts with
95 several of these small proteins. For example, the small adaptor protein PipX, a co-activator of the
96 global transcriptional regulator NtcA, is bound to PII in N replete conditions and is released upon

97 N limitation to form a complex with NtcA bound to 2-OG, thereby co-activating NtcA [20].
98 Furthermore, we showed recently the 51 amino acid protein PirA to antagonize functions of PII by
99 binding PII in an ADP-dependent manner and in turn preventing activation of N-acetylglutamate
100 kinase [21].

101 The 2,3-bisphosphoglycerate-independent phosphoglycerate-mutase (PGAM) reaction, which
102 converts the first CO_2 fixation product 3-phosphoglycerate (3-PGA) to 2-phosphoglycerate (2-
103 PGA), represents another major control point of the C/N balance that also involves the PII protein
104 [22]. The activity of PGAM determines the route of newly fixed carbon. In particular, C is taken out
105 from the CBB cycle and redirected towards lower glycolysis, supplying the carbon skeleton for
106 important anabolic reactions in amino acid, nucleic acid and lipid metabolism. PGAM activity is
107 controlled by the interaction with the 112 amino acid protein PirC (**P**II-**i**nteracting **r**egulator of
108 **c**arbon metabolism; *sll0944* product, which has also been termed CfrA [23]). PirC itself is under
109 control of the PII protein [22,24]. Under N replete conditions, hence low 2-OG levels, PirC is
110 sequestered by PII and inactive. When the N supply becomes limiting, the cellular 2-OG levels
111 increase, leading to the PII-ATP-2OG conformation, which releases PirC from the PII protein
112 complex. In turn, free PirC binds to and inhibits the activity of PGAM, thereby slowing the
113 conversion of 3-PGA to 2-PGA, which triggers the rapid synthesis of glycogen through activation
114 of GlgC by increasing 3-PGA levels [25]. Similarly, overexpression of the *pirC* gene caused rapid
115 accumulation of glycogen under vegetative conditions [23]. These results highlight the PirC-PGAM
116 switch as a pivot point for controlling the carbon flow in cyanobacterial metabolism.

117 Compared to classical metabolic engineering, focusing on the introduction of novel pathways,
118 targeting regulators for the intracellular re-modulation of metabolic fluxes is less prevalent but also
119 emerging in cyanobacteria [6,7,26]. Here, we engineered the cyanobacterial model strain
120 *Synechocystis* sp. PCC 6803 by tuning the PirC-PGAM switch and provide a proof of concept, by
121 modulating the components PGAM and PirC, to reach the maximum flux either into the direction

122 of acetyl-CoA (PGAM valve open, i.e. PGAM-ON state) or into gluconeogenic direction (PGAM
123 valve closed, i.e. PGAM-OFF state). The PGAM-ON state was achieved via overexpression of the
124 *pgam* gene, deleting the *pirC* gene or a combination of both. Under conditions of nitrogen
125 starvation, the PGAM-ON state led to excretion of metabolites from lower glycolysis, such as
126 pyruvate, 2-OG and succinate and to increased accumulation of PHB, proving the redirection of
127 carbon-flow towards lower glycolysis. Moreover, a PGAM-ON state in a recombinant strain also
128 expressing a plant-derived isoprene synthase led to increased production of isoprene under N
129 deprivation. Conversely, a PGAM-OFF state was established through inducible *pirC*
130 overexpression combined with *pgam* downregulation. Carbon flux redirection was evidenced by
131 increased glycogen accumulation, and optimized configurations were applied to enhance sucrose
132 production in salt-stressed *Synechocystis*. After induction, PGAM-OFF strains accumulated more
133 glycogen compared to the wild type, and also showed elevated sucrose levels under high-salt
134 conditions.

135

136 Materials and Methods

137 *Strains and growth conditions*

138 *Synechocystis* sp. PCC 6803 was obtained from the Pasteur Culture Collection of Cyanobacteria
139 and used as the wild type strain. Cultivation was carried out in BG11 medium [27]. Experimental
140 cultures were adjusted to an OD_{750} of 0.4 and maintained at 28°C under continuous illumination
141 (~70–80 µmol photons m^{-2} s^{-1}), with shaking at 125 rpm. For BG11 agar plates, the medium was
142 supplemented with 20 mM sodium tris-(hydroxymethyl)-ethyl phosphonate buffer (pH 8.2) and
143 1.5% Bacto agar. When required, appropriate antibiotics were added to pre-cultures. For nitrogen
144 depletion experiments, cells were pre-grown in BG11 medium to an OD_{750} of 0.6–1.0, then washed
145 three times with nitrogen-free BG11 medium ($BG11^0$). For glycogen and sucrose measurement

146 during PGAM-OFF state, cultures were inoculated at an OD_{750} of 0.2 and cultivated in Cu^{2+}-free
147 BG11 with appropriate antibiotics. For induction of the PGAM-OFF state $CuSO_4$ was added to a
148 final concentration of 1 µM. The cultures were then cultivated at 30 °C, 150 rpm, ambient CO_2, 50
149 µmol photons m^{-2} s^{-1} and 70% relative humidity. *Escherichia coli* (*E. coli*) strains were cultured in
150 LB medium or on LB agar plates (10 g/L NaCl, 10 g/L tryptone, 5 g/L yeast extract) at 37 °C,
151 supplemented with the appropriate antibiotic when required.

152

153 ***Genetic engineering***

154 All plasmids used and generated in this study are given in **Table S1**, the obtained recombinant
155 strains are listed in **Table S2**. The oligonucleotides used for DNA amplification are given in **Table**
156 **S3**. To construct the pSEVA251-P_{J23101}::*pgam* plasmid, Gibson Assembly was used [28]. DNA
157 amplification was performed with Q5 High-Fidelity DNA Polymerase (NEB) (primer
158 NB042/045/046/047) using the pSEVA251 plasmid or genomic *Synechocystis* DNA as template.
159 For purification of PCR-products and plasmid isolation, the Monarch® DNA Gel Extraction Kit and
160 Monarch® Plasmid Miniprep Kit (NEB) were used, respectively. The pSEVA251-P_{J23119}::*pgam*
161 plasmid was constructed using the Q5 Site-Directed Mutagenesis Kit (NEB) (primer NB075/076).
162 Plasmids were checked via sequencing (Eurofins Genomics, Ebersberg, Germany). To construct
163 the pSEVA451-P_{petE}::*pirC* plasmid a restriction-ligation approach was used. For this, the
164 respective promoter and gene sequences were amplified from the *Synechocystis* gDNA with
165 primers adding the recognition sites of the restriction enzymes used (FH013/017/018/019) and
166 fused by PCR (FH013/019). The fused gene construct was introduced into a pJET plasmid
167 (CloneJET PCR Cloning Kit, Thermo Fisher Scientific, Darmstadt) and excised from it using *Eco*RI
168 and *Bam*HI. The gene construct was then ligated into a pSEVA451 plasmid digested with the
169 same enzymes using T4 ligase (Thermo Fisher Scientific, Darmstadt). For purification of PCR-
170 products and plasmid isolation the NucleoSpin Gel and PCR clean-up Kit (Macherey-Nagel,

171 Düren) and the NucleoSpin Plasmid Mini Kit (Macherey-Nagel, Düren) were used, respectively.
172 The pEX-K248-P_{petJ}_*pgam* plasmid was synthesized by Eurofins. Plasmids were checked via
173 sequencing (Genewiz, Azenta Life Sciences, South Plainfield NJ).

174 The plasmids pSEVA251-P_{J23101}::*pgam* and pSEVA451-P_{petE}::*pirC* were introduced into
175 *Synechocystis* via electroporation as described [29], with minor modifications. To make
176 *Synechocystis* electrocompetent, 30 mL of culture in linear phase around OD_{750} 0.5 was collected
177 (4,000 g, 15 min, 4 °C). Cells were washed 3 times with 20 mL ice-cold HEPES (4-(2-
178 hydroxyethyl)-1-piperazineethanesulfonic acid) buffer (1 mM, pH 7.5). Then, cells were
179 resuspended in 1 mL HEPES and aliquots of 60 µL were either used directly or stored at -80 °C.
180 Electroporation was done with either 18.0 kV/cm or 2500 V for 5.2 ms, using 100-500 ng plasmid.
181 Cells were resuspended in 800 µL BG11 medium and plated onto BG11 agar plate without
182 antibiotics and incubated at 28 °C for one night before increasing the antibiotic concentration over
183 the next days. Clones were validated with colony PCR (primer NB062/063 or primer
184 FH017/019/076/081).

185 The P_{petJ}::*pgam* configuration was achieved by homologous recombination applying the pEX-
186 K248-P_{petJ}_*pgam* plasmid on naturally competent *Synechocystis*. For this, WT cells were collected
187 in their logarithmic growth phase at an OD_{750} of 0.5 to 1 by centrifugation at 3,000 x g for 5 min.
188 The supernatant was discarded and the cells were resuspended in BG11 (in 1% volume of initially
189 sampled material). Around 100 to 200 ng of DNA were added to 100 µL of concentrated cells,
190 mixed gently and incubated overnight at 30 °C in the dark and shaken at 150 rpm. Cells were
191 plated on BG11 with a low concentration of antibiotics and cultivated at 30 °C. Once colonies
192 appeared, they were picked onto plates with an increased concentration of antibiotics. Clones of
193 the *pgam_KD* strain were validated with colony PCR (FH011/020/027/101/102/111).

194 For the generation of isoprene producing *pirC* deletion strains, the isoprene production cassette
195 was amplified from plasmid pEERM3-2MEP-IspS:KmR via primers 2-MEP-PirCup_fw/rev. The

196 plasmid backbone was amplified with primers pEERM-PirCdwn_fw/pEERM-PirCup_rev. 500 bp
197 homology regions up- and downstream of *pirC* were generated with primers
198 PirCup_fw/PirCup_2MEP_rev and PirCwnd-2MEP_fw/PirCdwn_rev, respectively. The resulting
199 constructs were fused via AQUA cloning [30] and analogously used to obtain recombinant
200 *Synechocystis* strains.

201

202 ***Immunoblotting***

203 To analyze relative PGAM and PirC levels in recombinant *Synechocystis* strains, cells from 5-
204 10 mL culture were harvested by centrifugation at 4,000 x g for 15 min and the cell pellet was
205 stored at -20 °C until use. For cell lysis, the pellet was resuspended in 100 µL extraction buffer
206 (50 mM Tris-HCl, 5 mM EDTA, 100 µg/mL lysozyme (from chicken egg white), 1 µL/100 µL
207 protease inhibitor (Sigma Aldrich)). The samples were then incubated on ice for 1 hour. An equal
208 volume of glass beads (0.1-0.15 mm) was added for cell disruption using a FastPrep-24 Ribolyser
209 (MP Biomedicals) with five cycles of 15 s at 6.5 m/s and 4 °C. To load protein extracts on the SDS-
210 PAGE that correspond to equal volume of culture per lane, the samples were normalized to the
211 autofluorescence. This was done to correct different cell lysis efficiency, as well as drastic changes
212 in protein amounts in N-starved cells. The fluorescence of the cultures was measured immediately
213 before the cell harvest by a WATER-PAM chlorophyll fluorometer (Walz GmbH, Effeltrich,
214 Germany). The autofluorescence of the culture at time 0 was set in relation to the autofluorescence
215 measured at each time point of nitrogen-depletion. After lysis, the autofluorescence was measured
216 in the lysates and the same ratio as between the cultures was adjusted by correcting the volume
217 size with the following correction factor (see formula 1). For the control sample at time point 0,
218 ~10 µg protein per well were loaded, while for the samples in N starvation the correction factor
219 was used to calculate the volume accordingly.

220 $$correction\ factor\ f\ = \left(\frac{lysate\ \ \frac{t_0\ \ [F_0]}{t_x\ [F_0]}}{culture\ \frac{t_0\ \ [F_0]}{t_x\ [F_0]}} \right)$$

221 **Formula 1: Determination of the correction factor for SDS-PAGE sampling.** To determine the volume
222 of the SDS-PAGE sample, a correction factor (f) was determined using the ratio of the measured base
223 fluorescence (F_0) in the lysate normalized to the ratio of the fluorescence in the cell culture. The ratio thereby
224 represents the fluorescence at a time point x in chlorosis (t_x) to the control time point (before chlorosis, t_0).
225 F_0 = base fluorescence; t_0 = control time point (before chlorosis), t_x = time point x in chlorosis.

226

227 After measuring the autofluorescence of the lysates, the samples were centrifuged (16,000 g,
228 5 min, 4 °C) and the calculated volumes of lysate were boiled with SDS-loading dye (95 °C,
229 10 min). SDS-PAGE was performed as previously described [31], using 4-15% precast midi gels
230 (Q-PAGE). Western blotting was performed as previously described [32], using a methanol-
231 activated PVDF membrane (ROTI®PVDF 0.45). After protein transfer, the membrane was blocked
232 with 5% (w/v) milk powder in TBS-T buffer (50 mM Tris, 150 mM NaCl, 0.1% Tween-20, pH 7.4).
233 After washing with TBS-T buffer, the membrane was incubated with the primary antibody (PGAM
234 or PirC antiserum from rabbit, Davids Biotechnologie (see Appendix), 1:3,000 dilution in TBS-T)
235 for 1-2 h at RT, followed by a wash step. Then, the secondary antibody (antirabbit polyclonal goat
236 antibody–horseradish peroxidase conjugate; Sigma-Aldrich, 1:5,000 dilution in TBS-T) was
237 incubated for 1-2 h at RT or at 4 °C overnight, followed by a wash step. Immunoreactive bands on
238 the membrane were visualized using the LumiLight detection system (Roche Diagnostics) and the
239 Gel Logic 1500 imaging system (Kodak) with the respective software.

240

241 ***Metabolite profiling***

242 *Glycogen quantification*

243 Method A: Glycogen content was quantified using a colorimetric assay with *o*-dianisidine as
244 recently described [33]. Method B: Glycogen was additionally quantified by another colorimetric
245 method using *o*-toluidine adapted from [34]. For this, 2 mL of the cultures were centrifuged at
246 16,000 x g for 10 min. The pellet was washed twice with 1 mL MiliQ-water and suspended in 400
247 µL of KOH (30% (w/v)) and incubated at 95 °C for 2 h. Afterwards, 1.2 mL of ice-cold ethanol
248 (abs.) was added and glycogen was precipitated at -20 °C overnight. The samples were
249 centrifuged at 10,000 x g for 10 min and the supernatant was discarded. The cells were first
250 washed with 500 µL ethanol (70%) and then with 500 µL ethanol (abs.). The pellet was dried for
251 20 min at 60 °C in the Speed-Vac (Concentrator plus/Vacfuge plus®, Eppendorf, Wesseling-
252 Berzdorf). The dried pellet was taken up in 1 mL of 100 mM sodium acetate and 8 µL of
253 amyloglucosidase (4.4 U/µL) were added. The samples were incubated for 2 h at 60 °C. 200 µL
254 of the sample were mixed with 1 mL *o*-toluidine-reagent (6% in glacial acetic acid (v/v)) and
255 incubated at 100 °C for 10 min. Afterwards, the reaction was stopped by incubation on ice for 3
256 min. The measurement was done with 100 µL in a 96-well plate at 635 nm in a microwell-reader
257 (Infinite 200 PRO Reader, Tecan, Männedorf). As a standard, different glucose concentrations (1
258 mg/mL, 500 µg/mL, 250 µg/mL, 125 µg/mL, 62.5 µg/mL, 31.25 µg/mL and 0 µg/mL), also
259 incubated with *o*-toulidine-reagent as described above, were used.

260 *PHB quantification*

261 PHB was quantified with HPLC as described before [35], with the minor change that 10 mL cell
262 cultures were harvested and cell pellets were dried at 60 °C until the supernatant evaporated.

263 *Sucrose quantification*

264 For sucrose quantification, 2 mL cultures were centrifuged at 16,000 x g for 10 min and the cell
265 pellet was stored at -20 °C. Sucrose was extracted adapting a strategy from literature [36]. The

266 pellet was taken up in pre-cooled 80% ethanol. The cells were transferred into lysis tubes with
267 glass beads (Precellys® Aufschluss-Kit, Bertin technologies, Montigny-le-Bretonneux) and lysed
268 using a homogenizer (Precellys® evolution, Bertin technologies, Montigny-le-Bretonneux) and
269 afterwards incubated at 55 °C for 10 min. The suspension was centrifuged at 12,000 x g for 45
270 min and transferred to a fresh 2 mL tube. The ethanol was evaporated in a Speed-Vac
271 (Concentrator plus/Vacfuge plus®, Eppendorf, Wesseling-Berzdorf) at 30 °C for 2 h. The pellet
272 was taken up in 200 µL of MiliQ water. Sucrose was measured using a Vanquish HPLC system
273 (Thermo Scientific, Waltham) system equipped with an HiPlex H column (300 mm x 7.7mm x 8µm,
274 Agilent, Santa Clara) and a refractive index detector. Water at a flowrate of 0.6 ml/min was used
275 as the eluent. Column temperature was 15°C. As a standard, sucrose (Applichem, Darmstadt) at
276 1 mM, 0.5 mM, 0.25 mM, 0.125 mM, 0.0625mM and 0.03125 mM in MilliQ water was used.

277 *Quantification of extracellular metabolites*

278 Extracellular pyruvate, succinate, 2-oxoglutarate and glutamic acid concentrations were analyzed
279 with HPLC-MS from cell-free supernatant as described previously [33]. As standard, 0.01, 0.05
280 and 0.1 mM of sodium pyruvate ($C_3H_3NaO_3$, Sigma-Aldrich), sodium succinate dibasic
281 hexahydrate ($NaOOCCH_2CH_2COONa \cdot 6\ H_2O$, Sigma-Aldrich) and α-ketoglutaric acid disodium
282 salt hydrate (2-OG, $C_5H_4O_5Na_2 \cdot xH_2O$, Fluka Analytical) were used.

283 *Assessment of isoprene production*

284 For determining isoprene production, 20 mL of seed culture without antibiotics was transferred to
285 60 mL air-tight vials (Fisherbrand cat. no. 11540585) and cultivated at 40°C, 80 µmol photons m^{-}
286 ^{2} s^{-1} and 150 rpm for 1-15 h. For isoprene quantification, 150 µL of headspace were injected in a
287 gas chromatograph (Clarus 580, Perkin Elmer, Waltham, USA) equipped with a flame-ionisation
288 detector and a Porapak QS packed column (Porapak QS 80/80 PE 8000, 1.8 m × 2 mm ID, Cat.
289 No. N9305013-ZW5531, Perkin Elmer). Oven temperature was set to 200°C for 2.5 min with N_2 at

290 20 mL min^{-1} as carrier gas. Isoprene elution peaked at 1.74 min and was quantified based on the
291 peak area and synthetic standards. OD_{750} was determined after sampling.

292 Results

293 To demonstrate the potential of regulatory engineering to re-direct carbon-flow towards desired
294 product formation in cyanobacteria, we have generated *Synechocystis* strains with modified
295 PGAM valves. Two different directions of carbon-flow have been considered. For the synthesis of
296 products derived from lower glycolysis, the PGAM valve must be maximally open (PGAM-ON). To
297 synthesize products, derived from the upper part of central carbon metabolism (sugars, glycerol),
298 the PGAM valve has to be completely closed (PGAM-OFF). To achieve these states, we
299 modulated the abundance of either PGAM or PirC (**Fig. 1**).

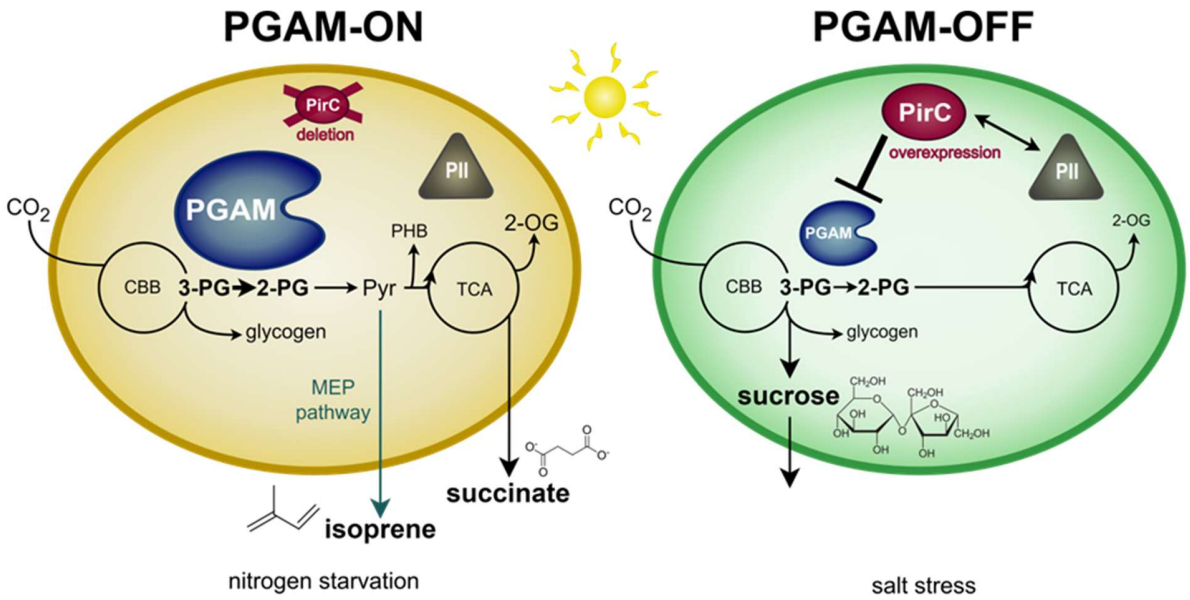

300

301 **Figure 1: Illustration of the basic principle of engineering the PirC-PGAM-valve.** In *Synechocystis*, the
302 PGAM-PirC switch tightly regulates the carbon flow at the branching point between upper and lower
303 glycolysis. In this case study, the aim is to direct the carbon flow either towards lower glycolysis (succinate
304 and isoprene excretion), by overexpressing PGAM to decrease the inhibition of PirC under nitrogen

305 starvation (PGAM-ON state, left panel) or towards gluconeogenesis (sucrose production), by engineering a
306 strong inhibition of PGAM by PirC (PGAM-OFF state, right panel).

307

308 ***Regulatory engineering towards the PGAM-ON state in* Synechocystis**

309 A potential PGAM-ON state requires high basal PGAM activity, which might be obtained by
310 increasing enzyme abundance via overexpression of the *pgam* gene. To achieve the PGAM-ON
311 state, *Synechocystis* strains were generated that ectopically express the *pgam* gene driven by
312 constitutive synthetic promoters (BioBricks BBa), either J23101 for moderate or J23119 for strong
313 overexpression, similar to previous studies [37,38] (**Fig. 2A**). These plasmids were introduced into
314 *Synechocystis* WT and into a strain lacking the *pirC* gene [22], which therefore lacks the inhibition
315 of PGAM by PirC. Finally, we obtained the strains 101_*pgam*, 119_*pgam* and Δ*pirC* + 101_*pgam*,
316 which were verified by colony PCR (see **Fig. S1A-C**), and we performed immunoblotting using a
317 PGAM-specific antiserum. As expected, when *pgam* gene expression was driven by either
318 PJ23101 or PJ23119, strong PGAM accumulation was achieved compared to the WT or Δ*pirC*
319 control strains (**Fig. 2B**). In addition to vegetative growth conditions, we also analyzed cells grown
320 under nitrogen starvation as *pgam* gene expression was reported to be downregulated in nitrogen-
321 starved cells, according to the microarray analysis shown in [39]. However, PGAM overproduction
322 in the engineered strains was not affected by nitrogen starvation and remained stably high even
323 after 14 d in nitrogen starvation (**Fig. S1D**). Under either condition, the expression driven by the
324 J23119 promoter led to higher PGAM abundance compared to the J23101 promoter, which is in
325 agreement with previously reported promoter strength [37]. Contrary to its interaction target, PirC
326 is increased under nitrogen starvation (**Fig. 2B**), which is in agreement with previous reports
327 [39,40]. Interestingly, we observed a correlation between increased PGAM abundance in strains
328 101_*pgam* and 119_*pgam* and an increase of PirC (**Fig. 2B**) even though the *pirC* gene
329 expression was not genetically manipulated in these strains. The PGAM-dependent accumulation

330 of PirC might be a response to counteract a redirection of carbon flow towards lower glycolysis
331 albeit the mechanism behind this remains unclear.

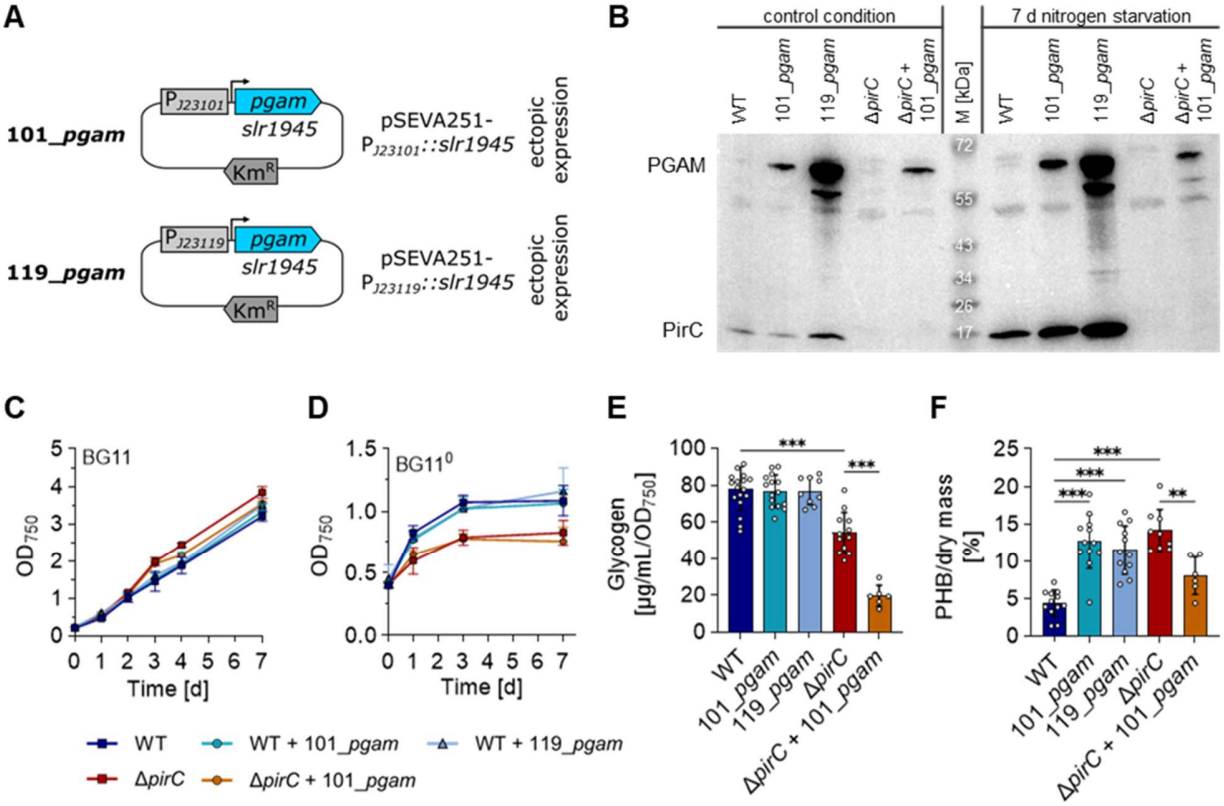

332

333 **Figure 2: Demonstration of the PGAM-ON state. A:** Plasmid design for overexpressing the native *pgam*
334 gene (*slr1945*) from the pSEVA251 plasmid under control of the moderate J23101 or strong J23119
335 promoter. **B:** Immunoblots against PGAM and PirC for cells grown under vegetative (control) conditions and
336 for 7 days under N starvation. **C-D:** Vegetative growth (C) and OD_{750} under nitrogen starvation (D) with at
337 least three biological replicates. **E-F:** Quantification of glycogen with method A (E) and PHB (F) after 7 days
338 of N starvation. Each dot represents a biological replicate. Dunn's multiple comparisons test was used (ns
339 = P > 0.05, * = P ≤ 0.05, ** = P ≤ 0.01, *** = P≤ 0.001).

340

341 After detecting higher PGAM levels in the *pgam* overexpressing strains, we analyzed if the
342 established genetic configurations might affect growth performance of *Synechocystis*. As

343 compared to the corresponding reference strains, neither the presence of pSEVA251 nor the
344 overexpression of *pgam* had a significant impact on growth performance under vegetative or
345 nitrogen-depleted conditions (**Fig. 2C, D** & **Fig. S2**). As already reported previously, upon
346 nitrogen-downshift the Δ*pirC* mutant didn't show the final doubling before arresting growth that
347 *Synechocystis* usually does, but showed a premature growth arrest [22,24]. The Δ*pirC* +
348 101_*pgam* strain behaved in the same way as the Δ*pirC* strain.

349 Previous studies showed that a Δ*pirC* mutant, i.e. a strain lacking the proteinaceous inhibitor of
350 PGAM, produces less glycogen and more PHB under nitrogen starvation compared to the WT
351 [22]. However, under this uninhibited condition, the amount of PGAM might still be the limiting
352 factor of carbon flow. To evaluate this, we made a similar experiment as Orthwein et al. (2021)
353 using the generated *pgam* overexpression strains and analyzed glycogen and PHB contents after
354 7 days of N starvation (**Fig. 2E, F**). Indeed, the *pgam* overexpression altered the carbon flow, but
355 with different outcome in either WT or Δ*pirC* background. In the WT background, glycogen content
356 was not significantly altered by higher PGAM levels, neither in the 101_*pgam* nor in the 119_*pgam*
357 strain (**Fig. 3E**). However, both PGAM overproduction strains produced around 12% PHB per dry
358 mass, which was three times more than detected in the WT (~4%) and the same as in the Δ*pirC*
359 mutant (~14%) (**Fig. 3F**). In contrast, the Δ*pirC* + 101_*pgam* strain formed significantly less
360 glycogen compared to the Δ*pirC* reference strain (~2.5 times less) and PHB production was
361 reduced by almost half (8%). The combined effect of *pirC* deletion and *pgam* overexpression might
362 imbalance cell metabolism more drastically than the *pirC* deletion alone.

363

364 ***Regulatory engineering towards the PGAM-OFF state in* Synechocystis**

365 To achieve the PGAM-OFF state, we aimed at diminishing *pgam* gene expression combined with
366 an overexpression of the *pirC* gene to change the equilibrium towards increased amounts of the
367 PirC-PGAM complex (see **Fig. 1**). This, in turn, would result in inhibited flux towards acetyl-CoA

368 and would boost the yields of products derived from gluconeogenesis, such as sucrose. For this,
369 we fused the corresponding genes with promoters that are controlled by micromolar
370 concentrations of copper ions [41], i.e. the *pirC* gene with the *petE* promoter (P*petE*) and the *pgam*
371 gene with the *petJ* (P*petJ*) promoter, to achieve this scenario upon Cu^{2+} addition (**Fig. 3A**). The
372 obtained construct P*petE*::*pirC* was introduced into *Synechocystis* WT on a replicative plasmid.
373 However, the construct P*petJ*::*pgam* was introduced into the chromosome of *Synechocystis,*
374 thereby replacing the native *pgam* gene locus (**Fig. 3A**). The obtained strains for Cu^{2+}-inducible
375 *pgam* knockdown (pgam_KD) or *pirC* overexpression (pirC_OEX) were genetically confirmed
376 (**Fig. 3B**). In addition, a strain that combined both the pgam_KD and the pirC_OEX constructs was
377 designed. Subsequently, all strains were analyzed regarding growth performance to estimate any
378 pleiotropic effects caused by the changed genetic configuration, but none of the configurations did
379 affect growth compared to the WT (**Fig. 3 C-E**). Finally, glycogen accumulation was also tracked
380 in the mutant strains (**Fig. 3 F-H**). Both the pgam_KD and the pirC_OEX strain accumulate
381 glycogen after supplementation with 1 µM copper sulfate, while the glycogen amount within the
382 cultures before induction was comparable to the WT. In particular, strain pgam_KD showed a 6-
383 fold increase of glycogen compared to the WT at 48 h after diminishing *pgam* gene expression
384 (**Fig. 3F**). The effect was more drastic in strain pirC_OEX and levels around 400 µg/mL/OD_{750} at
385 48 h after induction, while almost no glycogen was detectable in the WT (**Fig. 3G**). The
386 combination of both pgam_KD and pirC_OEX also showed an increased glycogen concentration
387 compared to the WT after addition of Cu^{2+}, while the glycogen concentration before the induction
388 with Cu^{2+} was comparable to the WT. However, the effect that could be seen here was not as
389 drastic as the effect of the pirC_OEX on its own and accompanied with rather high biological
390 variation (**Fig. 3H**).

391

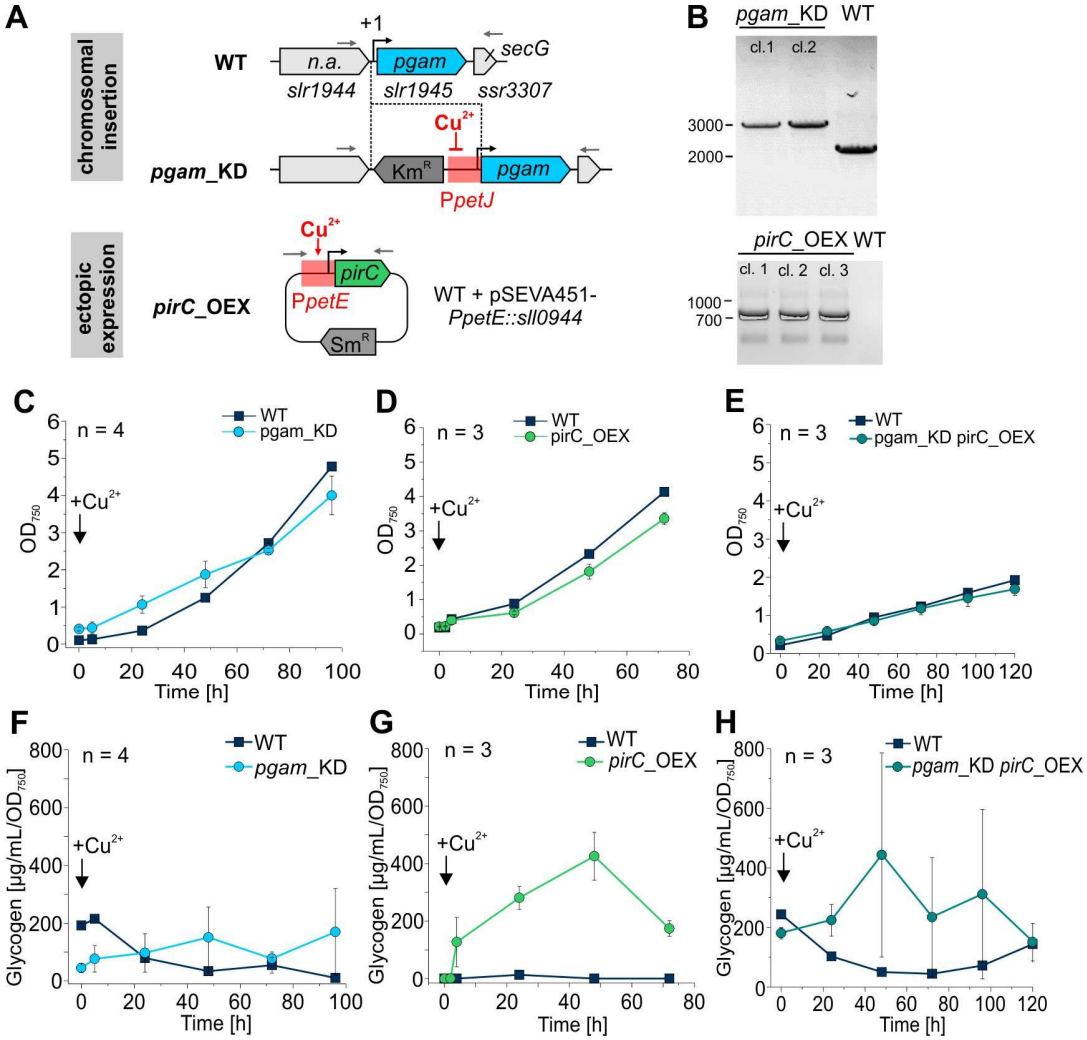

392

393 **Figure 3: *Synechocystis* strains with genetic configurations demonstrating the PGAM-OFF state**. **A:**
394 Design of constructs to achieve *pirC* overexpression and *pgam* downregulation using copper controllable
395 promoters from *Synechocystis.* **B:** Verification of recombinant strains. The obtained strains were verified by
396 PCR, using primer combinations illustrated by grey arrows in panel A. **C-E:** Growth of the different mutants
397 pgam_KD and pirC_OEX and the combination mutant of pgam_KD and pirC_OEX compared to the wildtype
398 under inducing conditions, i.e in presence of Cu^{2+} at a final concentration of 1 µM. **F-H:** Development of the
399 average glycogen amount in the obtained strains compared to the WT after the addition Cu^{2+} at a final
400 concentration of 1 µM. Glycogen was measured using method B. Data are the mean ± SD of n biological
401 replicates as indicated.

402

403 ***The PGAM-ON state enhances the production of succinate - a representative of the***
404 ***lower glycolysis route***

405 First of all, the engineered PGAM-ON strains, i.e. those with a modulated carbon flow towards the
406 TCA cycle, were analyzed regarding metabolites known to be excreted from *Synechocystis*.
407 Pyruvate, 2-OG and succinate were reported to be released to the medium under nitrogen
408 depletion, especially when the carbon flow has been altered [33,42,43]. Therefore, extracellular
409 concentrations of these metabolites were quantified in the supernatant of cell cultures that have
410 been N-starved for 7 days using HPLC-MS. Under the conditions used in this study, pyruvate
411 could not be detected in the supernatant of WT cultures under N starvation, similar to previous
412 studies [43]. However, overexpression of *pgam* resulted in increased pyruvate secretion, as in
413 both strains 101_*pgam* and 119_*pgam,* pyruvate was detectable in a range between 2-3 mg/L
414 (**Fig. 4A**). The Δ*pirC* mutant excreted even more pyruvate, which, however, was not further
415 elevated when the *pgam* gene was ectopically expressed. The supernatant of both strains, Δ*pirC*
416 and Δ*pirC*+101_*pgam*, contained ~4 mg/L pyruvate (**Fig. 4A**). Similar effects were also observed
417 for 2-OG. While ~1.5 mg/L 2-OG were detected in the medium of WT cultures, strains 101_*pgam*
418 and 119_*pgam* excreted 7-fold and 9-fold higher 2-OG levels compared to the WT, respectively
419 (**Fig. 4B**). Deletion of *pirC* resulted in approximately 20 times higher 2-OG concentrations in the
420 medium, reaching around 28 mg/L, which again did not further increase when *pgam*
421 overexpression was also established.

422 The TCA cycle intermediate succinate was also quantified. The WT strain released 0.3 mg/L
423 succinate to the medium after cultivation for 7 days under N starvation. Again, the established
424 PGAM-ON state resulted in increased succinate excretion compared to the WT (**Fig. 4C**). Strains
425 101_*pgam* and 119_*pgam* showed comparable succinate levels of between 0.8 and 1.3 mg/L.
426 Accordingly, overexpression of the *pgam* gene resulted in 2- to 4-fold higher succinate excretion.
427 This became much more drastic in the Δ*pirC* strain, which accumulated 5-6 mg/L and hence,

428 18-fold higher succinate levels compared to the WT (**Fig. 4C**). As seen for the other quantified
429 metabolites, additional *pgam* overexpression in Δ*pirC* could not significantly enhance succinate
430 excretion.

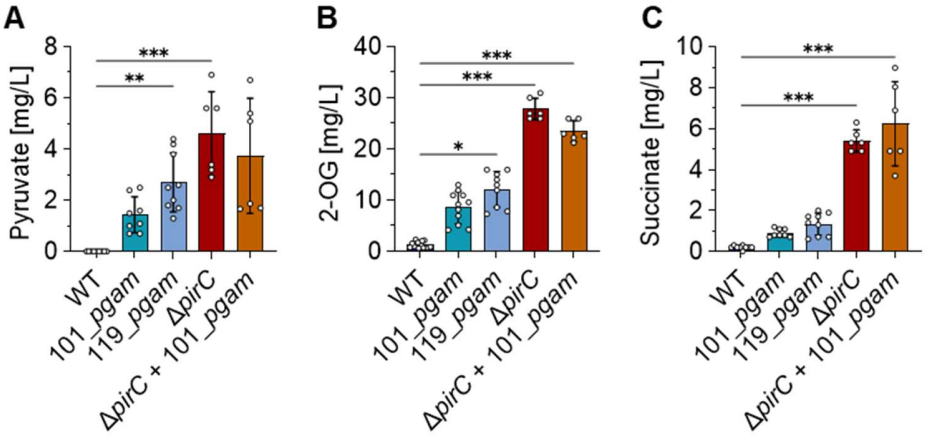

431

432 **Figure 4: Making use of the PirC-PGAM-switch to form certain products from lower glycolysis, e.g.**
433 **succinate.** Pyruvate (A), 2-OG (B) and succinate (C) were quantified with HPLC-MS from the supernatant
434 of 7-day N-depleted cell cultures. Each dot represents a biological replicate. Dunn's multiple comparisons
435 test was used (ns = P > 0.05, * = P ≤ 0.05, ** = P ≤ 0.01, *** = P≤ 0.001).

436

437 ***An opened PGAM valve enhances heterologous production of isoprene***

438 In addition to succinate, which is of biotechnological interest itself [44], we analyzed if the here
439 established genetic configurations, targeting the PGAM valve, also enhance the production of
440 other pyruvate-derived compounds of economic importance. For example, the hydrocarbon
441 isoprene is not naturally produced by *Synechocystis* but can be generated from precursors of the
442 non-mevalonate (MEP) pathway by introducing plant-derived isoprene synthases [45] (**Fig. 5A**).
443 To test the effect of an open PGAM valve on isoprene production, a gene cassette enabling
444 isoprene production was introduced into the *pirC* gene locus via homologous recombination,
445 thereby replacing the native *pirC* gene (**Fig. 5B**). For comparison, a previously published
446 production strain [46] was used, that carries the same isoprene production cassette in ORF

447 *slr0168*, which is dispensable for *Synechocystis* under standard growth conditions and hence
448 considered as neutral integration site (defined as neutral site I (NSI)) (**Fig. 5B**). Here, absence of
449 *pirC* did not have significant effects on growth or isoprene formation under standard conditions
450 (**Fig. 5C, D**), however, 24 hours after induction of N starvation, strong differences in the isoprene
451 output were observed (**Fig. 5E**), pointing towards an open PGAM valve that upholds carbon flux
452 into MEP. Nevertheless, isoprene formation ceased entirely after 3 days, pointing towards
453 complete metabolic arrest under these conditions (not shown). Moreover, volumetric productivity
454 was substantially lower when compared to N-replete conditions, given that growth was arrested
455 entirely, consistent with previous reports.

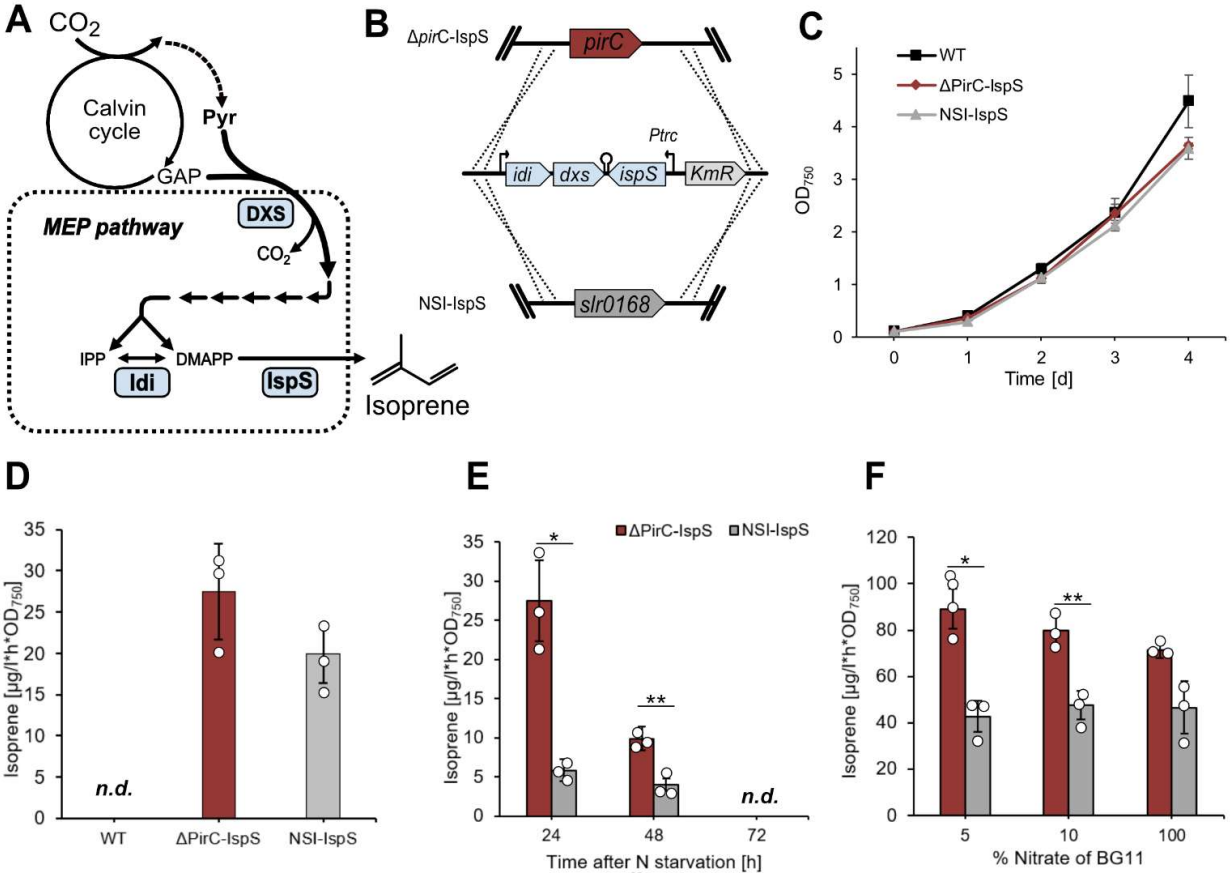

456

457 **Figure 5: Isoprene formation upon *pirC* deletion in engineered *Synechocystis* strains. A:** Simplified
458 scheme of metabolic framework for MEP-pathway derived isoprene production, overproduced enzymes in
459 production strains are marked in blue. *Coleus forskohlii* D-xylulose-5-phosphate synthase (DXS),

460 *Synechocystis* isopentenyl pyrophosphate isomerase (Idi), *Eucalyptus globulus* isoprene synthase (IspS)
461 **B:** Genetic constructs enabling isoprene production in *Synechocystis* and concomitant deletion of *pirC* or
462 *slr0168*, respectively. **C:** Growth comparison during standard growth conditions. **D:** Specific isoprene
463 production activity after 3 days of cultivation at standard conditions. **E:** Specific isoprene production activity
464 in response to N starvation. **F:** Specific isoprene production activity after 24 hours of cultivation under
465 respective conditions. Data shown are average values and standard deviations of 3 biological replicates,
466 significance was tested using paired two samples Student's t-test (ns = $P > 0.05$, * = $P \leq 0.05$, ** = $P \leq 0.01$).

467

468 This shows that strict N starvation is not applicable for continuously high production levels. Thus,
469 to test the open PGAM valve under varying N availability, exponentially grown seed cultures were
470 washed with $BG11^0$ and subsequently cultivated in BG11 containing 5, 10 or 100% nitrate, with
471 the latter corresponding to regular BG11. After 24 hours, the open PGAM valve enabled similar
472 isoprene formation with 5 and 10% nitrate when compared to the control strain cultivated in 100%
473 N, indicating higher carbon flux towards pyruvate in the *pirC* knockout under N-limiting conditions
474 as compared to the wild-type (**Fig. 5F**).

475

476 ***Sucrose as representative of gluconeogenic routes: Closing the PGAM valve is***
477 ***boosting sucrose production***

478 Sucrose has been shown to accumulate as an osmotic compound to counteract high osmolarity,
479 e.g. in presence of mM concentrations of NaCl, which can be easily tolerated by *Synechocystis*
480 [47,48]. As the PGAM-OFF state increases the carbon flux towards gluconeogenesis, it should
481 enhance sucrose formation upon the addition of salt. First, we tested the impact of salt stress on
482 the strains' glycogen concentration in both the pgam_KD as well as the pgam_KD pirC_OEX
483 mutant before and after salt shock. The measurement before salt shock was done at 24 h after
484 induction with copper ions, while the measurement after salt shock was done after 120 h of

485 cultivation in salt. Both mutant strains accumulate glycogen during cultivation in medium with 500
486 mM NaCl. The pgam_KD mutant and pgam_KD pirC_OEX mutant accumulate about ten times
487 more glycogen than the WT (**Fig. 6 A,B**). To monitor sucrose accumulation, both the wild type and
488 the *pgam*_KD strain were subjected to salt shock and different time points after downregulating
489 *pgam* gene expression by copper sulfate were analyzed. For this, both the pgam_KD mutant and
490 the combination mutant of pgam_KD and pirC_OEX were compared to the wild type. All cultures
491 were induced with copper ions 24 h previous to the salt shock. While the pgam_KD mutant did not
492 accumulate more sucrose compared to the WT, the pgam_KD pirC_OEX mutant did accumulate
493 more than twice as much sucrose compared to the WT at 8 h after salt shock (**Fig. 6 C,D**).

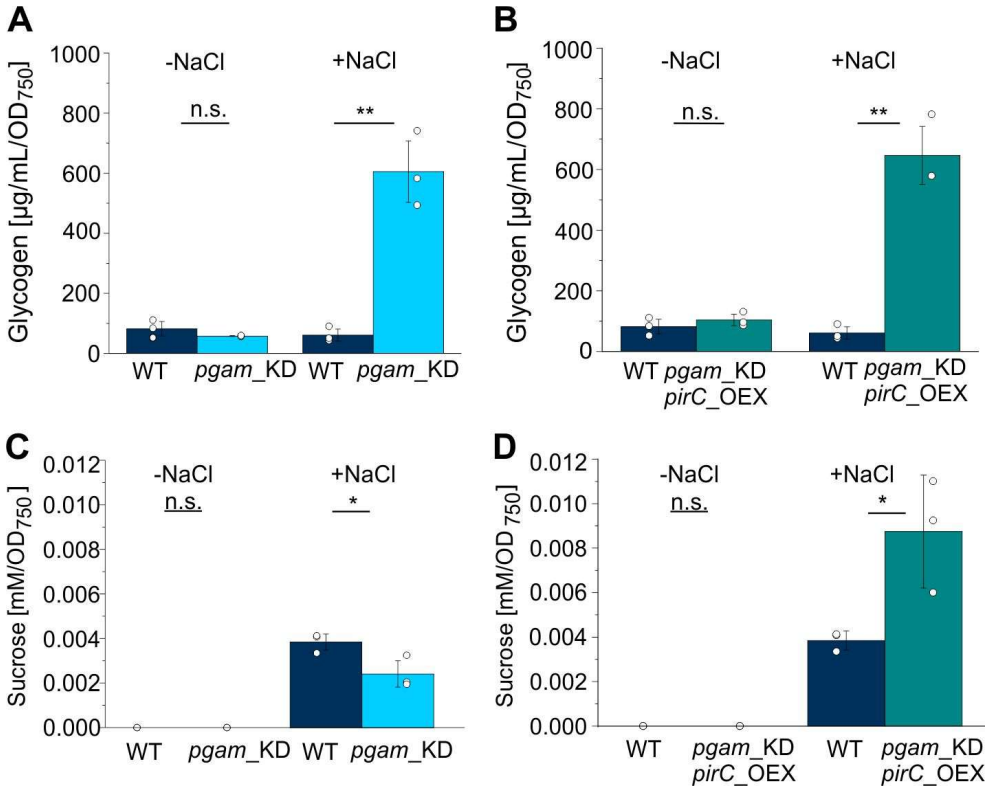

494

495 **Figure 6: Boosting salt-dependent sucrose formation by modulating the PirC-PGAM switch.** For
496 glycogen and sucrose measurements, cells were salt shocked 24 h after induction with copper ions. **A:**
497 Glycogen measurement in the pgam_KD mutant before and after salt shock. **B:** Glycogen measurement in
498 the pgam_KD pirC_OEX mutant before and after salt shock. Glycogen was measured using method B.

499 Measured concentrations are shown with respect to the liquid volume of the sampled cultures at
500 OD750. **C:** Sucrose content in the pgam_KD mutant at two time points before salt shock as well as 8 h
501 after salt shock. **D:** Sucrose content in the pgam_KD pirC_OEX mutant at two time points before and 8 h
502 after salt shock. Each dot represents a biological replicate. T-test was done for statistical analysis (ns = P >
503 0.05, * = P ≤ 0.05, ** = P ≤ 0.01, *** = P ≤ 0.001).

504

505 ## Discussion

506 The 2,3-bisphosphogylcerate-independent phosphoglycerate mutase (PGAM) activity determines
507 whether fixed carbon is retained in gluconeogenic routes supporting glycogen and sucrose
508 synthesis or is directed toward pyruvate, acetyl-CoA, and the TCA cycle. It therefore occupies a
509 strategic position at the interface of the CBB cycle and lower glycolysis and hence, is tightly
510 regulated [22,23]. PGAM activity is controlled by the small protein PirC (also named CfrA in the
511 parallel studies of the Muro-Pastor group, [23]), which inhibits PGAM upon release from PII under
512 nitrogen starvation [22]. Previous work has demonstrated that this key regulatory node has
513 significant influence on cellular carbon allocation and hence is also an attractive target for
514 metabolic engineering [49–52].

515 In this study, we demonstrate systematic engineering of the PGAM-PirC regulatory node, which
516 represents an effective strategy to redirect central carbon flux in *Synechocystis* toward both native
517 and heterologous products, which is a clear extension to previous studies. By rationally modulating
518 PGAM activity, either by opening or closing the PGAM valve, we established two distinct metabolic
519 states: PGAM-ON and PGAM-OFF, that enable preferential routing of carbon into lower glycolysis
520 or gluconeogenesis, respectively. Importantly, this strategy operates at the level of native
521 metabolic regulation rather than by introducing irreversible pathway blocks, preserving cellular
522 flexibility while enabling productive flux redirection.

523 To establish the PGAM-ON state, *pgam* was overexpressed using two promoters of different
524 strengths (J23101 and J23119). Under vegetative conditions, increased PGAM abundance did
525 not affect growth, consistent with PGAM reaching equilibrium independently of PirC, which is
526 sequestered by PII. During nitrogen starvation, PirC is released and inhibits PGAM [22], promoting
527 glycogen accumulation. However, PGAM overexpression partially counteracted this inhibition and
528 redirected carbon toward lower glycolysis. As a result, PGAM-ON strains exhibited increased PHB
529 accumulation and a 2-3-fold enhancement in excretion of TCA-cycle-derived metabolites
530 compared to the wild type. Although PGAM overexpression partially counteracts this inhibition,
531 our data indicate that PirC levels are concomitantly upregulated. The reason for this remains
532 elusive. The observed increase in excreted metabolites such as succinate, pyruvate, and 2-
533 oxoglutarate is notable given that wild-type *Synechocystis* releases only trace amounts of organic
534 acids during chlorosis. This highlights the tight endogenous control of metabolite excretion and
535 underscores the effectiveness of PGAM overexpression in overcoming this constraint. The results
536 are consistent with previous studies showing elevated intracellular pools of these metabolites in
537 strains with impaired PirC-mediated regulation [22,33].

538 Deletion of *pirC* has an even more pronounced effect on carbon allocation. In the Δ*pirC* mutant,
539 PGAM is no longer inhibited during nitrogen starvation, leading to a strong redirection of carbon
540 toward lower glycolysis and the TCA cycle. We show that this metabolic shift not only increases
541 PHB accumulation, as previously reported [49], but also results in substantial excretion of organic
542 acids, particularly 2-oxoglutarate. Given the central role of 2-oxoglutarate in C/N sensing via PII
543 [8], its excretion likely reflects a compensatory response to severe metabolic imbalance. The fact
544 that overexpression of PGAM in the Δ*pirC* background does not further increase metabolite
545 excretion suggests that the system has already reached a new equilibrium, beyond which
546 additional PGAM no longer enhances efflux from the CBB cycle.

547 Among the excreted metabolites, succinate is of particular biotechnological interest, as it is listed
548 among the top platform chemicals from biomass by the US Department of Energy. *Synechocystis*
549 WT does not excrete succinate under standard photoautotrophic conditions [43], and previous
550 efforts to induce succinate production have relied on deleting carbon sinks such as glycogen
551 synthesis or by disrupting succinate dehydrogenase [53,54]. Our data demonstrate that
552 engineering the PGAM-ON state alone is sufficient to induce succinate excretion, without directly
553 targeting succinate metabolism. This finding positions the PGAM-PirC valve as a complementary
554 strategy that can be combined with established metabolic interventions. For example, coupling
555 the PGAM-ON state with deletion of *sdhB* or introduction of a glyoxylate shunt by expressing an
556 isocitrate lyase from *E. coli* [55] may further enhance succinate yields. In addition, PHB synthesis
557 represents a major acetyl-CoA sink during nitrogen starvation, and its removal could increase
558 carbon availability for organic acid production. Thus, PGAM valve engineering provides a versatile
559 entry point for multi-layered optimization strategies.

560 Conversely, establishment of a PGAM-OFF state through inducible *pirC* overexpression and/or
561 *pgam* downregulation redirected carbon flux toward gluconeogenesis. All PGAM-OFF strains
562 showed an increase in glycogen accumulation, with glycogen levels peaking approximately 48 h
563 after induction. The strongest effect was observed in our *pirC* overexpression strain, which
564 accumulated glycogen to levels exceeding those previously reported when using analogous
565 genetic configurations based on arsenite-inducible promoters [51]. Beyond glycogen, we explored
566 how the PGAM-OFF state affects sucrose metabolism. Sucrose serves as a compatible solute
567 during salt stress and is metabolically linked to glycogen in *Synechocystis* [48]. When PGAM-OFF
568 strains were subjected to salt shock, both glycogen and sucrose accumulation were enhanced
569 compared to the wild type, although the magnitude of the effect depended on the specific genetic
570 configuration. In particular, the combined *pgam* knockdown/*pirC* overexpression strain exhibited
571 a clear increase in sucrose accumulation, supporting the idea that stronger control over PGAM

572 activity translates into more pronounced flux redirection. These findings align well with recent work
573 demonstrating enhanced sucrose production by controlling carbon flux through CfrA (= PirC)
574 overproduction in *Synechocystis* [52]. Together, these studies reinforce the concept that
575 regulatory control points upstream of sucrose biosynthesis can be leveraged to increase
576 compatible solute production without directly modifying the sucrose synthesis pathway itself.
577 Combining PGAM-OFF engineering with established strategies such as overexpression of the
578 gene of the sucrose phosphate synthase or deletion of the invertase gene [56,57] is therefore a
579 promising route toward further yield improvements.

580 In addition to native products, we demonstrated that PGAM valve engineering can also improve
581 production of heterologous compounds such as isoprene, derived from pyruvate. Consistent
582 observations have been made in recombinant *Synechocystis* strains optimized for ethanol
583 production [50]. This highlights the broader applicability of this approach for pathways branching
584 from central metabolism. Notably, recent work has identified a PGAM variant with higher activity
585 and reduced sensitivity to PirC inhibition [24], suggesting that future efforts could further decouple
586 PGAM activity from endogenous regulatory feedback and expand the dynamic range of the valve.

587 Conclusions

588 Overall, our study establishes the mechanism controlling the PGAM valve as a powerful tool that
589 can be modulated in *Synechocystis* for controlling carbon flux in a customized manner. By fine-
590 tuning a native regulatory mechanism, we enable flexible redistribution of carbon rather than
591 imposing irreversible pathway blocks that might have further negative effects. More broadly, these
592 findings underscore the potential of small regulatory proteins as engineering targets for metabolic
593 rewiring as suggested previously [19]. The PGAM-PirC valve thus provides a strong foundation
594 for future photosynthesis-driven biotechnological applications and for integrating regulatory
595 engineering with pathway-level optimization.

Declarations

Ethics approval and consent to participate

Not applicable

Consent for publication

Not applicable

Availability of data and materials

All data generated or analyzed during this study are included in this published article and its supplementary information files.

Competing interests

The authors declare that they have no competing interests

Funding

We acknowledge individual funding by the Deutsche Forschungsgemeinschaft (grants KL 3114/7-1 obtained by S.K. and FO 195/22-1 obtained by K.F.).

Authors' contributions

SK and KF designed the study. NSB, FH, PB, KO, TO, AK and PF performed research. NSB drafted the manuscript. FH, KF, PB, PL and SK reviewed and edited the manuscript. All authors proof-read the final manuscript and agreed with publication.

Acknowledgements

We thank Ron Stauder for technical support. ChatGPT was used for language editing of selected manuscript sections, in particular the abstract and parts of the discussion.

617 ## References

618 1. Hohmann-Marriott MF, Blankenship RE. Evolution of photosynthesis. Annu Rev Plant Biol.
619 2011;62:515–48. https://doi.org/10.1146/annurev-arplant-042110-103811

620 2. Falkowski PG, Fenchel T, Delong EF. The microbial engines that drive Earth's biogeochemical
621 cycles. Science. 2008;320:1034–9. https://doi.org/10.1126/science.1153213

622 3. Ducat DC, Way JC, Silver PA. Engineering cyanobacteria to generate high-value products.
623 Trends Biotechnol. 2011;29:95–103. https://doi.org/10.1016/j.tibtech.2010.12.003

624 4. Angermayr SA, Gorchs Rovira A, Hellingwerf KJ. Metabolic engineering of cyanobacteria for
625 the synthesis of commodity products. Trends Biotechnol. 2015;33:352–61.
626 https://doi.org/10.1016/j.tibtech.2015.03.009

627 5. Toepel J, Karande R, Klähn S, Bühler B. Cyanobacteria as whole-cell factories: current status
628 and future prospectives. Curr Opin Biotechnol. 2023;80:102892.
629 https://doi.org/10.1016/j.copbio.2023.102892

630 6. Bolay P, Dodge N, Janssen K, Jensen PE, Lindberg P. Tailoring regulatory components for
631 metabolic engineering in cyanobacteria. Physiol Plant. 2024;176:e14316.
632 https://doi.org/10.1111/ppl.14316

633 7. Klähn S, Opel F, Hess WR. Customized molecular tools to strengthen metabolic engineering of
634 cyanobacteria. Green Carbon. 2024;2:149–63. https://doi.org/10.1016/j.greenca.2024.05.002

635 8. Forchhammer K, Selim KA. Carbon/nitrogen homeostasis control in cyanobacteria. FEMS
636 Microbiol Rev. 2020;44:33–53. https://doi.org/10.1093/femsre/fuz025

637 9. Forchhammer K, Selim KA, Huergo LF. New views on PII signaling: from nitrogen sensing to
638 global metabolic control. Trends Microbiol. 2022;S0966-842X(21)00321-8.
639 https://doi.org/10.1016/j.tim.2021.12.014

640 10. Huergo LF, Dixon R. The Emergence of 2-Oxoglutarate as a Master Regulator Metabolite.
641 Microbiol Mol Biol Rev. 2015;79:419–35. https://doi.org/10.1128/MMBR.00038-15

642 11. Forchhammer K, Lüddecke J. Sensory properties of the PII signalling protein family. FEBS J.
643 2016;283:425–37. https://doi.org/10.1111/febs.13584

644 12. Espinosa J, Forchhammer K, Burillo S, Contreras A. Interaction network in cyanobacterial
645 nitrogen regulation: PipX, a protein that interacts in a 2-oxoglutarate dependent manner with P_{II}
646 and NtcA. Mol Microbiol. 2006;61:457–69. https://doi.org/10.1111/j.1365-2958.2006.05231.x

647 13. Espinosa J, Rodríguez-Mateos F, Salinas P, Lanza VF, Dixon R, de la Cruz F, et al. PipX, the
648 coactivator of NtcA, is a global regulator in cyanobacteria. Proc Natl Acad Sci USA.
649 2014;111:E2423-2430. https://doi.org/10.1073/pnas.1404097111

650 14. Heinrich A, Maheswaran M, Ruppert U, Forchhammer K. The *Synechococcus elongatus* P
651 signal transduction protein controls arginine synthesis by complex formation with N-acetyl-L-
652 glutamate kinase. Mol Microbiol. 2004;52:1303–14. https://doi.org/10.1111/j.1365-
653 2958.2004.04058.x

654 15. Maheswaran M, Urbanke C, Forchhammer K. Complex Formation and Catalytic Activation by
655 the PII Signaling Protein of N-Acetyl-l-glutamate Kinase from *Synechococcus elongatus* Strain
656 PCC 7942. J Biol Chem. 2004;279:55202–10. https://doi.org/10.1074/jbc.M410971200

657 16. Hauf W, Schmid K, Gerhardt ECM, Huergo LF, Forchhammer K. Interaction of the nitrogen
658 regulatory protein GlnB (PII) with biotin carboxyl carrier protein (BCCP) controls acetyl-CoA levels
659 in the cyanobacterium *Synechocystis* sp. PCC 6803. Front Microbiol. 2016;7:1700.
660 https://doi.org/10.3389/fmicb.2016.01700

661 17. Steinberg R, Koch H-G. The largely unexplored biology of small proteins in pro- and
662 eukaryotes. FEBS J. 2021; https://doi.org/10.1111/febs.15845

663 18. Baumgartner D, Kopf M, Klähn S, Steglich C, Hess WR. Small proteins in cyanobacteria
664 provide a paradigm for the functional analysis of the bacterial micro-proteome. BMC Microbiol.
665 2016;16:285. https://doi.org/10.1186/s12866-016-0896-z

666 19. Brandenburg F, Klähn S. Small but Smart: On the Diverse Role of Small Proteins in the
667 Regulation of Cyanobacterial Metabolism. Life (Basel). 2020;10.
668 https://doi.org/10.3390/life10120322

669 20. Espinosa J, Forchhammer K, Contreras A. Role of the *Synechococcus* PCC 7942 nitrogen
670 regulator protein PipX in NtcA-controlled processes. Microbiology (Reading). 2007;153:711–8.
671 https://doi.org/10.1099/mic.0.2006/003574-0

672 21. Bolay P, Rozbeh R, Muro-Pastor MI, Timm S, Hagemann M, Florencio FJ, et al. The novel
673 PII-interacting protein PirA controls flux into the cyanobacterial ornithine-ammonia cycle. mBio.
674 2021;12. https://doi.org/10.1128/mBio.00229-21

675 22. Orthwein T, Scholl J, Spät P, Lucius S, Koch M, Macek B, et al. The novel PII-interactor PirC
676 identifies phosphoglycerate mutase as key control point of carbon storage metabolism in
677 cyanobacteria. Proc Natl Acad Sci U S A. 2021;118. https://doi.org/10.1073/pnas.2019988118

678 23. Muro-Pastor MI, Cutillas-Farray Á, Pérez-Rodríguez L, Pérez-Saavedra J, Vega-de Armas A,
679 Paredes A, et al. CfrA, a Novel Carbon Flow Regulator, Adapts Carbon Metabolism to Nitrogen
680 Deficiency in Cyanobacteria. Plant Physiol. 2020;184:1792–810.
681 https://doi.org/10.1104/pp.20.00802

682 24. Orthwein T, Alford JT, Becker NS, Fink P, Forchhammer K. Structural elements of
683 cyanobacterial co-factor-independent phosphoglycerate mutase that mediate regulation by PirC.
684 mBio. 2025;16:e03378-24. https://doi.org/10.1128/mbio.03378-24

685 25. Lee K, Doello S, Hagemann M, Forchhammer K. Deciphering the tight metabolite-level
686 regulation of glucose-1-phosphate adenylyltransferase (GlgC) for glycogen synthesis in
687 cyanobacteria. FEBS J. 2025;292:759–75. https://doi.org/10.1111/febs.17348

688 26. Watzer B, Engelbrecht A, Hauf W, Stahl M, Maldener I, Forchhammer K. Metabolic pathway
689 engineering using the central signal processor PII. Microb Cell Fact. 2015;14:192.
690 https://doi.org/10.1186/s12934-015-0384-4

691 27. Rippka R, Deruelles J, Waterbury JB, Herdman M, Stanier RY. Generic assignments, strain
692 histories and properties of pure cultures of cyanobacteria. J Gen Microbiol. 1979;111:1–61.
693 https://doi.org/10.1099/00221287-111-1-1

694 28. Gibson DG, Young L, Chuang R-Y, Venter JC, Hutchison CA, Smith HO. Enzymatic assembly
695 of DNA molecules up to several hundred kilobases. Nat Methods. 2009;6:343–5.
696 https://doi.org/10.1038/nmeth.1318

697 29. Ludwig A, Heimbucher T, Gregor W, Czerny T, Schmetterer G. Transformation and gene
698 replacement in the facultatively chemoheterotrophic, unicellular cyanobacterium Synechocystis
699 sp. PCC6714 by electroporation. Appl Microbiol Biotechnol. 2008;78:729–35.
700 https://doi.org/10.1007/s00253-008-1356-y

701 30. Beyer HM, Gonschorek P, Samodelov SL, Meier M, Weber W, Zurbriggen MD. AQUA Cloning:
702 A versatile and simple enzyme-free cloning approach. PLoS ONE. 2015;10:e0137652.
703 https://doi.org/10.1371/journal.pone.0137652

704 31. Schägger H. Tricine-SDS-PAGE. Nat Protoc. 2006;1:16–22.
705 https://doi.org/10.1038/nprot.2006.4

706 32. Towbin H, Staehelin T, Gordon J. Electrophoretic transfer of proteins from polyacrylamide gels
707 to nitrocellulose sheets: procedure and some applications. Proc Natl Acad Sci U S A.
708 1979;76:4350–4. https://doi.org/10.1073/pnas.76.9.4350

709 33. Alford JT, Becker NS, Rapp J, Kulik A, Kaewbai-Ngam J, Monshupanee T, et al. Controlled
710 carbon loss: Threshold-dependent overflow metabolism in *Synechocystis* sp. PCC 6803.
711 Microorganisms. 2025;13:2767. https://doi.org/10.3390/microorganisms13122767

712 34. Gründel M, Scheunemann R, Lockau W, Zilliges Y. Impaired glycogen synthesis causes
713 metabolic overflow reactions and affects stress responses in the cyanobacterium *Synechocystis*
714 sp. PCC 6803. Microbiology (Reading). 2012;158:3032–43. https://doi.org/10.1099/mic.0.062950-
715 0

716 35. Fink P, Menzel C, Kwon J-H, Forchhammer K. A novel recombinant PHB production platform
717 in filamentous cyanobacteria avoiding nitrogen starvation while preserving cell viability. Microb
718 Cell Fact. 2025;24:43. https://doi.org/10.1186/s12934-025-02650-y

719 36. Hoehnel A, Salas García J, Coffey C, Zannini E, Arendt EK. Comparative study of sugar
720 extraction procedures for HPLC analysis and proposal of an ethanolic extraction method for plant-
721 based high-protein ingredients. J Sci Food Agric. 2022;102:5055–64.
722 https://doi.org/10.1002/jsfa.11204

723 37. Vasudevan R, Gale GAR, Schiavon AA, Puzorjov A, Malin J, Gillespie MD, et al. CyanoGate:
724 A Modular Cloning Suite for Engineering Cyanobacteria Based on the Plant MoClo Syntax. Plant
725 Physiol. 2019;180:39–55. https://doi.org/10.1104/pp.18.01401

726 38. Itzenhäuser MA, Enkerlin AM, Dewald JA, Avşar B, Stauder R, Halpick H, et al. Deciphering
727 guanidine assimilation and riboswitch-based gene regulation in cyanobacteria for synthetic biology
728 applications. Proc Natl Acad Sci U S A. 2025;122:e2519335122.
729 https://doi.org/10.1073/pnas.2519335122

730 39. Klotz A, Georg J, Bučinská L, Watanabe S, Reimann V, Januszewski W, et al. Awakening of
731 a dormant cyanobacterium from nitrogen chlorosis reveals a genetically determined program. Curr
732 Biol. 2016;26:2862–72. https://doi.org/10.1016/j.cub.2016.08.054

733 40. Spät P, Klotz A, Rexroth S, Maček B, Forchhammer K. Chlorosis as a developmental program
734 in cyanobacteria: The proteomic fundament for survival and awakening. Mol Cell Proteomics.
735 2018;17:1650–69. https://doi.org/10.1074/mcp.RA118.000699

736 41. García-Cañas R, Giner-Lamia J, Florencio FJ, López-Maury L. A protease-mediated
737 mechanism regulates the cytochrome c6/plastocyanin switch in *Synechocystis* sp. PCC 6803.
738 Proc Natl Acad Sci U S A. 2021;118. https://doi.org/10.1073/pnas.2017898118

739 42. Namakoshi K, Nakajima T, Yoshikawa K, Toya Y, Shimizu H. Combinatorial deletions of *glgC*
740 and *phaCE* enhance ethanol production in *Synechocystis* sp. PCC 6803. J Biotechnol.
741 2016;239:13–9. https://doi.org/10.1016/j.jbiotec.2016.09.016

742 43. Kato Y, Hidese R, Matsuda M, Ohbayashi R, Ashida H, Kondo A, et al. Glycogen deficiency
743 enhances carbon partitioning into glutamate for an alternative extracellular metabolic sink in
744 cyanobacteria. Commun Biol. 2024;7:233. https://doi.org/10.1038/s42003-024-05929-9

745 44. Bechthold I, Bretz K, Kabasci S, Kopitzky R, Springer A. Succinic Acid: A New Platform
746 Chemical for Biobased Polymers from Renewable Resources. Chemical Engineering &
747 Technology. 2008;31:647–54. https://doi.org/10.1002/ceat.200800063

748 45. Lindberg P, Park S, Melis A. Engineering a platform for photosynthetic isoprene production in
749 cyanobacteria, using *Synechocystis* as the model organism. Metab Eng. 2010;12:70–9.
750 https://doi.org/10.1016/j.ymben.2009.10.001

751 46. Rana A, Gomes LC, Rodrigues JS, Yacout DMM, Arrou-Vignod H, Sjölander J, et al. A
752 combined photobiological–photochemical route to C10 cycloalkane jet fuels from carbon dioxide
753 via isoprene. Green Chem. The Royal Society of Chemistry; 2022;24:9602–19.
754 https://doi.org/10.1039/D2GC03272D

755 47. Klähn S, Hagemann M. Compatible solute biosynthesis in cyanobacteria. Environ Microbiol.
756 2011;13:551–62. https://doi.org/10.1111/j.1462-2920.2010.02366.x

757 48. Kirsch F, Klähn S, Hagemann M. Salt-regulated accumulation of the compatible solutes
758 sucrose and glucosylglycerol in cyanobacteria and its biotechnological potential. Front Microbiol
759 [Internet]. 2019 [cited 2021 Mar 22];10. https://doi.org/10.3389/fmicb.2019.02139

760 49. Koch M, Bruckmoser J, Scholl J, Hauf W, Rieger B, Forchhammer K. Maximizing PHB content
761 in *Synechocystis* sp. PCC 6803: a new metabolic engineering strategy based on the regulator
762 PirC. Microb Cell Fact. 2020;19:231. https://doi.org/10.1186/s12934-020-01491-1

763 50. Böhm J, Kauss K, Michl K, Engelhardt L, Brouwer E-M, Hagemann M. Impact of the carbon
764 flux regulator protein pirC on ethanol production in engineered cyanobacteria. Front Microbiol.
765 2023;14:1238737. https://doi.org/10.3389/fmicb.2023.1238737

766 51. Domínguez-Lobo MT, Roldán M, Gutiérrez-Diánez AM, Florencio FJ, Muro-Pastor MI. Double
767 blocking of carbon metabolism causes a large increase of Calvin-Benson cycle compounds in
768 cyanobacteria. Plant Physiol. 2024;195:1491–505. https://doi.org/10.1093/plphys/kiae083

52. Domínguez-Lobo MT, Ortega-Martínez P, Florencio FJ, Muro-Pastor MI. Enhanced sucrose production by controlling carbon flux through CfrA expression in *Synechocystis* sp. PCC 6803. Microb Cell Fact. 2025; https://doi.org/10.1186/s12934-025-02894-8

53. Mock M, Schmid A, Bühler K. Photoautotrophic production of succinate via the oxidative branch of the tricarboxylic acid cycle influences glycogen accumulation in *Synechocystis* sp. PCC 6803. Algal Research. 2019;43:101645. https://doi.org/10.1016/j.algal.2019.101645

54. Mock M, Schmid A, Bühler K. Directed reaction engineering boosts succinate formation of *Synechocystis* sp. PCC 6803_Δ*sll1625*. Biotechnol J. 2020;15:e2000127. https://doi.org/10.1002/biot.202000127

55. Durall C, Kukil K, Hawkes JA, Albergati A, Lindblad P, Lindberg P. Production of succinate by engineered strains of *Synechocystis* PCC 6803 overexpressing phosphoenolpyruvate carboxylase and a glyoxylate shunt. Microb Cell Fact [Internet]. 2021 [cited 2021 Mar 22];20. https://doi.org/10.1186/s12934-021-01529-y

56. Du W, Liang F, Duan Y, Tan X, Lu X. Exploring the photosynthetic production capacity of sucrose by cyanobacteria. Metab Eng. 2013;19:17–25. https://doi.org/10.1016/j.ymben.2013.05.001

57. Kirsch F, Luo Q, Lu X, Hagemann M. Inactivation of invertase enhances sucrose production in the cyanobacterium *Synechocystis* sp. PCC 6803. Microbiology (Reading). 2018;164:1220–8. https://doi.org/10.1099/mic.0.000708

58. Silva-Rocha R, Martínez-García E, Calles B, Chavarría M, Arce-Rodríguez A, de Las Heras A, et al. The Standard European Vector Architecture (SEVA): a coherent platform for the analysis and deployment of complex prokaryotic phenotypes. Nucleic Acids Res. 2013;41:D666-675. https://doi.org/10.1093/nar/gks1119